Overtone and combination features of G and D peaks in resonance Raman spectroscopy of the $C_{78}H_{26}$ polycyclic aromatic hydrocarbon

A. Maghsoumi,[a] L. Brambilla,[a] C. Castiglioni,[a] K. Müllen[b] and M. Tommasini[a]*

Introduction

Polycyclic aromatic hydrocarbons (PAHs) have inspired scientific research for several reasons. They have provided models to develop and test elementary π-bond theory.[1] The extended π-conjugation and self-organizing properties of PAHs are important properties for molecular electronics.[2] Their carcinogenic activity is of concern because PAHs occur as intermediate combustion products upon soot formation.[3] Furthermore, PAHs are organic molecular species present in interstellar space, and they represent an important research field in astrophysics.[4]

It is well-known that Raman spectroscopy is a convenient probe for analyzing PAHs[5–7] and graphenes[8] because, it is fast, is non-destructive, provides structural and electronic information, and can be adopted not only in academic laboratories but also, as a perspective, for the characterization of materials in industrial production frameworks.

The Raman spectroscopy of graphene, graphite and PAHs has been extensively investigated.[5–10] The first-order Raman spectra of these materials show a characteristic pattern constituted by two strong bands located at around 1600 cm^{-1} and 1300 cm^{-1}. For PAHs these Raman signals are also structured, i.e. they show several components. These signals are characteristic of sp^2 carbon materials and have been traditionally called G and D bands, respectively.

The D band (from 'disorder') appears in graphitic systems when some kind of disorder or discontinuity of the lattice occurs. Raman features in the D region are also observed in amorphous carbon systems with mixed sp^2/sp^3 content.[11] In PAHs the D peak is an intrinsic Raman signal that can be taken as signature of the confinement of π electrons and relaxation of the molecular structure with respect to the equalized CC bonds characteristic of graphene/graphite. It is worth considering that the Raman investigation of PAHs (as oligomers of graphene) can provide information that could be used for a better characterization of graphene itself. Obviously, since the advent of graphene,[12,13] this point may disclose important practical applications. For instance this kind of a situation occurred in the past, when the origin of the Raman D peak was debated[7,14,15] and the right early assignment of the phonon dispersion curves of graphene was the result of calculations originated from molecular models[10,16,17] later confirmed by first principles calculations.[18]

We may expect a similar situation here, because the D peak overtone in the Raman spectra of graphene and few layer graphenes is routinely used to characterize the quality of the materials produced.[8] However, even though a connection of the G and D peaks in graphene and PAHs does exist,[7] as far as the authors are aware of, the same cannot be said for the higher order Raman processes, such as 2D or 2G. This work is a first attempt to dwell more into this issue, by considering in details the Raman spectra of $C_{78}H_{26}$ (**C78**, for short—see Fig. 1) including overtones and combinations, and the dependence of the spectra with respect to the excitation wavelength.

On one side we have carried out a series of experiments in order to determine the Raman behavior of **C78** taken as representative model of D_{2h} PAHs. On the other side we have provided an interpretation of the experimental data by means of calculations of the Raman response, including overtones and combinations, which is based upon Density Functional Theory (DFT) and Nafie–Peticolas–Stein theory of resonant Raman.[19,20] Compared with

* *Correspondence to: Matteo Tommasini, Dip. Chimica, Materiali, Ing. Chimica, Politecnico di Milano, Italy.*
E-mail: matteo.tommasini@polimi.it

a *Dipartimento di Chimica, Materiali ed Ingegneria Chimica 'G. Natta', Politecnico di Milano, Italy*

b *Max Planck Institute for Polymer Research, Ackermannweg 10, D-55128, Mainz, Germany*

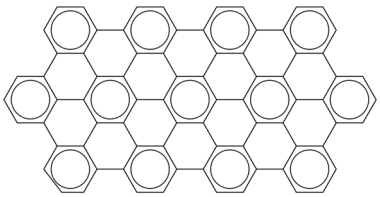

Figure 1. Molecular structure of **C78**, a PAH belonging to the D_{2h} point group. Clar's aromatic sextets are evidenced.

previous investigation of resonance Raman response of PAHs[6,7] the present method allows a substantial computational saving, because it does not require the optimization of the excited states. A resonance Raman approach has to be adopted because for **C78** with the excitations wavelengths adopted by us (785, 632.8, 514.5, 457.9 and 325 nm) we match electronic resonance conditions.[6,21]

Because **C78** represents a confined graphitic structure exhibiting peculiar G + D Raman combination signals, the results presented here could be useful to characterize with Raman spectroscopy other confined graphene systems such as graphene islands[22–25] or graphene ribbons.[26,27]

Experimental and theoretical methods

The powder of **C78**, already investigated in the past,[6] was synthesized as described by Watson *et al*.[21] To improve the quality of the Raman spectra, in this work we have repeatedly washed the sample with tetrahydrofuran (THF) in which **C78** is insoluble. This allowed reducing effectively the fluorescence background signal thus easing the collection of the weaker Raman features. The **C78** powder (about 2 mg) was dispersed in THF (about 3 ml) and sonicated for 15 min, hence centrifuged for 10 min at 5000 RPM. Then 2 ml of surnatant was removed and replaced with fresh THF. Thereafter the dispersion was sonicated again, and the whole procedure was repeated 3 times. The cleaned **C78** powder was recovered after complete evaporation of residual THF.

The Raman spectra presented here have been recorded with a Jobin-Yvon Labram HR800UV spectrometer. Different laser lines have been used, namely 325 nm (He–Cd laser), 457.9 and 514.5 nm (Ar^+ laser), 632.8 nm (He–Ne laser) and 785 nm (high power diode laser). The laser power at the sample was always of the order of a few mW to prevent (or reduce as possible) laser-induced effects on the samples; care has been adopted to verify the reproducibility of the spectra. Samples were analyzed in a back-scattering geometry on glass slides by using the microscope with the 50× objective for all laser lines except the one at 325 nm for which an UV-grade 15× objective was used. The intensity of all reported Raman spectra (325 nm excitation excluded) have been corrected with white light calibration.

The Linkam THMS600 stage was used for temperature-dependent Raman spectra starting from room temperature (RT) and increasing stepwise by 25 °C up to 200 °C. The Raman spectra were recorded in correspondence of each temperature step, allowing the sample to reach a stable equilibrium temperature.

We have modeled the Raman response of **C78** by means of DFT calculations carried out at the B3LYP/6-31G** level. At first, we have computed the off-resonance Raman spectra with the standard procedure available within the selected quantum chemistry code (Gaussian09 D.01[28]). When comparing experimental data with computed peak wavenumber we adopted a scaling factor of 0.9793 that has been adopted so to fit the position of the G peak in the simulated and experimental spectra. We have then evaluated the resonance Raman response of **C78** adopting the theoretical approach introduced by Nafie, Stein and Peticolas[19] which is discussed in details in[20] where it is applied to π conjugated systems (polyenes). It requires the calculation of the gradient at the Franck–Condon point on the potential energy surface of the excited state of interest. We adopted a Time-Dependent DFT (TDDFT) approach (B3LYP/6-31G**) to evaluate the gradient. From it, the electron–phonon coupling parameters of all normal modes can be determined, and the relative intensities of first-order Raman processes, overtones and combinations can be evaluated.[20][1] In the present treatment we have considered perfect resonance conditions with selected excited states of **C78** (namely S_1, S_4 and S_6). Based on our calculation we have analyzed the experimental spectra recorded with different excitations and rationalized the observed spectra in the low wavenumber, D, G, overtone and combination regions.

The chosen theoretical approach for the evaluation of resonance Raman has the benefit of requiring a limited computational effort, compared to more accurate treatments[29] of resonance Raman which can deal in more details with Raman excitation profiles and non-totally symmetric normal modes (see Section on Low Wavenumber Region). The consideration of the computational effort is particularly relevant in molecular graphenes, which are usually sizeable systems.

Discussion of the Raman spectra

Before addressing the experimental Raman spectra of **C78**, it is worth describing briefly the nature of the main Raman signals of PAHs, which are named G and D after their analogy with the corresponding Raman signals of graphene/graphite systems.

Graphite's G band (from 'graphite') is assigned to the degenerate $\mathbf{q} = \mathbf{0}$ (where **q** is the phonon wave vector) optical phonon of E_{2g} symmetry of the graphene lattice.[10] Because, compared with graphene, point group symmetry lowers in **C78** and becomes D_{2h} (see Fig. 1), the modes of the molecule which correspond to the degenerate G modes of graphene may formally belong to either A_g or B_{3g} irreducible representation. For A_g modes the nuclear displacements of the molecular core (i.e. the seven innermost condensed rings) occur along the long molecular axis, while for B_{3g} modes occur along the short molecular axis (see Fig. 2 and Table S1 (Supporting Information)). However, it is worth noticing that the totally symmetric modes are significantly stronger than the B_{3g} modes (this is expected in Raman spectroscopy, see also Table S1 (Supporting Information)). Hence the G peak of **C78** mainly features longitudinal modes.

The Raman intensity of the D peak is vanishing by symmetry in graphene, and it becomes sizeable only because of translational symmetry breaking (e.g. by the presence of defects/edges in the graphene flake, or by confinement of π electrons in finite size PAHs —see for instance[7,8,30]). The D peak is assigned to a specific vibrational mode that can be described as a cooperative breathing of alternated hexagonal rings in the core of the molecule[6,9] (see Fig. 3).

To simplify the discussion of the Raman spectra we divide the analysis in three sections, namely (a) the medium wavenumber region comprising the D, G signals (1000 – 1800 cm^{-1}), (b) the low

[1]The present approach does compute the Raman intensities of fundamentals, overtones and combinations within the harmonic approximation of the potential energy surface. Hence the assessment of the anharmonic effects of Fermi and Darling–Dennison resonances[33] in the simulated spectra is not straightforward within this theoretical framework.

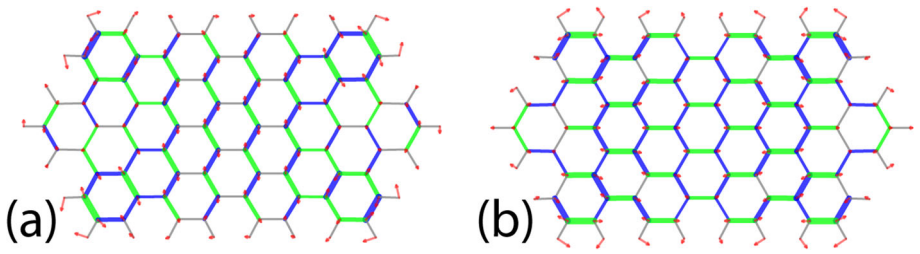

Figure 2. Representation of selected G-peak normal modes of **C78**: (a) transversal B_{3g} mode computed at 1643 cm^{-1}; (b) longitudinal A_g mode computed at 1635 cm^{-1}. Results from B3LYP/6-31G** calculations. Red arrows represent displacement vectors; CC bonds are represented as green (blue) lines of different thickness according to their relative stretching (shrinking).

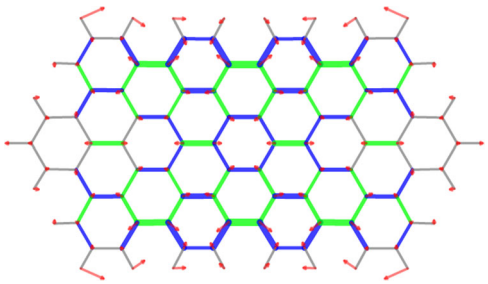

Figure 3. Representation of the D-peak normal mode of **C78** computed at 1294 cm^{-1} (B3LYP/6-31G** calculation). It is worth noticing that the rings corresponding to Clar's sextets in Fig. 1 are those involved in the collective breathing vibration, which is a characteristic feature of the modes in the D region. Red arrows represent displacement vectors; CC bonds are represented as green (blue) lines of different thickness according to their relative stretching (shrinking).

wavenumber region (<1000 cm^{-1}) and (c) the high wavenumber region (1800–3500 cm^{-1}) featuring overtone and combination lines. The temperature dependence of the G peak will be discussed in the ending paragraph of this section.

(a) **D, G region**. The experimental Raman spectra of **C78** excited with several laser lines are presented in Fig. 4. It is evident that the Raman spectra in this region are significantly sensitive to the variation of the excitation energy. Between 1150 cm^{-1} and 1450 cm^{-1} at least 11 D peaks (D_1–D_{11}) are observed, whose relative intensities are highly sensitive to the excitation wavelength. The positions of D_1–D_{11} are reported in Table 1 based on deconvolution of spectra (details are given in Fig. S1 (Supporting Information)). Within experimental error and band convolution uncertainty the position of these components is expected to be independent with respect to the laser excitation (as can be judged in Table 1). This is because of the assignment of each D component to a specific molecular normal mode. The relative intensity of the most distinguished peaks in the D region redistributes to the higher wavenumber transitions by increasing the laser excitation energy. In particular, the relative intensity of the D_2–D_3–D_4 triplet (collectively labeled D_{low}) compared with the quintuplet D_5–D_6–D_7–D_8–D_9 (collectively labeled D_{high}) decreases by increasing the laser excitation energy: the D_{low} dominates the D-region with the 632.8 nm excitation while the D_{high} dominates with 457.8 and 325 nm; excitations (see Fig. S2 (Supporting Information) for the quantitative D_{low}/D_{high} intensity ratio behavior as a function of excitation wavelength). The lowest wavenumber peak observed in the D region (D_1, 1170 cm^{-1}) is not particularly strong; however its relative intensity is significantly enhanced going form 325 nm to 785 nm laser excitation.

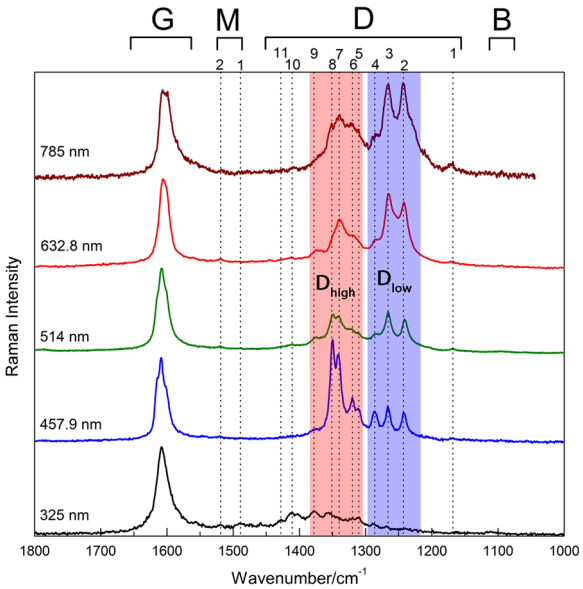

Figure 4. Comparison between experimental Raman spectra of **C78** recorded with different laser wavelengths.

Simulations of Raman spectra of **C78** in perfect resonance with the low lying bright exited states (S_1, S_4, S_6—see Table S2 (Supporting Information)), which are reported in Fig. 5, allow rationalizing the observed intensity redistribution within the D region. The lower wavenumber tail of the D region is comparatively stronger in S_1 than it is in S_6. To obtain a more quantitative agreement of theoretical data with experiments (i.e. a fine peak assignment going beyond the identification of the strongest features in the D region) one would require (i) a better determination of the vibrational structure of the molecule and (ii) a more accurate determination of the excited states to get more reliable relative intensities. We think that for the typical spectroscopic practice and the present case, issue (i) may be slightly more important than (ii). Issue (i) is important because, given the spectral congestion of the D peak region, small changes in the description of the normal modes (e.g. going from a lower to a higher level of calculation) may already affect the simulated Raman profile, even keeping the Raman polarizability tensors of the lower level calculation.[2] Of course, this point just considers the shape of the Raman spectrum, not the value of the absolute Raman intensities

[2] One can see this effect as a sort of mode mixing, i.e. the modes computed at a higher level can be expressed as a linear combination of the modes computed at the lower level.

Table 1. Position of the main components of the Raman signal in the D region as a function of the laser excitation (from band deconvolution)

	325 nm	457.9 nm	514.5 nm	632.8 nm	785 nm
D_1	—	—	1168	1170	1170
D_2	1239	1241	1240	1242	1241
D_3	1268	1266	1266	1264	1267
D_4	1287	1286	1284	1286	1286
D_5	1310	1310	1310	—	1310
D_6	1320	1320	1324	1318	1322
D_7	1344	1341	1340	1339	1340
D_8	1357	1350	1350	1350	1350
D_9	1378	1378	1375	1374	1371
D_{10}	1409	1411	1412	1414	1409
D_{11}	1429	—	1428	—	1427

or the excitation dependence of the Raman spectrum, which are known to depend on issue (ii). Unfortunately **C78** is too large to allow, with present technology, the straightforward use of more accurate basis sets and/or quantum chemistry methods.

The experimental Raman spectra show a structured G-band; however, the shape of the G-band is less sensitive to the laser excitation energy compared to the D-band. As it is shown in Fig. 4, the spectra recorded with 457.9 nm and 514.5 nm excitations have a good signal-to-noise ratio in the G region and clearly show that the G signal is contributed by at least three overlapped peaks centered at 1601, 1609 and 1615 cm^{-1}. Within experimental error and band convolution uncertainty the position of these components is expected to be independent with respect to the laser excitation (as can be judged in Table 2). This is because of the assignment of each G component to a specific molecular normal mode. The analysis of DFT calculations (Table S1 (Supporting Information)) shows the presence of five modes with sizeable Raman activity in the G peak region. However, their wavenumbers are such that they cluster into three groups, which explains the number of peaks experimentally observed. Based on this observation the G-band has been deconvoluted taking into account three components for the

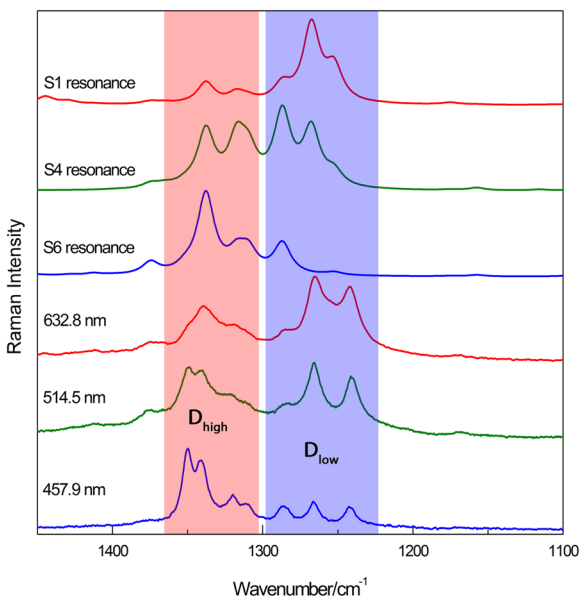

Figure 5. Comparison between calculated perfect resonances spectra and experimental spectra with different laser excitation in D region.

Table 2. Position of the three main components of the Raman signal in the G region as a function of the laser excitation (from band deconvolution)

	325 nm	457.9 nm	514.5 nm	632.8 nm	785 nm
G_1	1601	1601	1601	1601	1599
G_2	1609	1609	1609	1608	1608
G_3	—	1615	1615	—	—

457.9 and 514.5 nm excitations. For the other laser excitations (325, 632.8 and 785 nm) we have just considered two components, because the third one is too weak to allow for a reliable peak deconvolution. The summary of the experimental G peak data is reported in Table 2 (Fig. S3 (Supporting Information) shows the result of the peak deconvolution).

The relative intensity of the G *versus* the D region does depend significantly upon the laser excitation energy, as it can be judged by inspecting Fig. 4. Because of the presence of several D (and G) signals, we have considered the integrated area under the G and D regions. The I_D/I_G ratio so evaluated (Fig. S2 (Supporting Information)) increases as the laser photon energy decreases (i.e. going from 325 nm; to 785 nm excitation). This behavior parallels a similar observation made by Pócsik *et al.* on microcrystalline graphite.[31]

In addition to the main G and D features, the 1000–1800 cm^{-1} spectral range shows other minor Raman signals, which have been labeled B (breathing modes) and M (middle modes). They are, respectively, found at lower wavenumbers than the D band and in the middle between the G and D bands. B and M signals are very weak, but they can be observed with good reliability with green laser excitation and also find a match in DFT calculations (see Fig. S4 (Supporting Information) and Fig. S5 (Supporting Information) for details about the B and M regions).

(b) **Low wavenumber region.** The Raman spectra of **C78** recorded with 514.5 and 632.8 nm laser excitations are presented in Fig. 6 over the 130–1000 cm^{-1} range. The inset plot of Fig. 6 allows judging the sizeable relative intensity

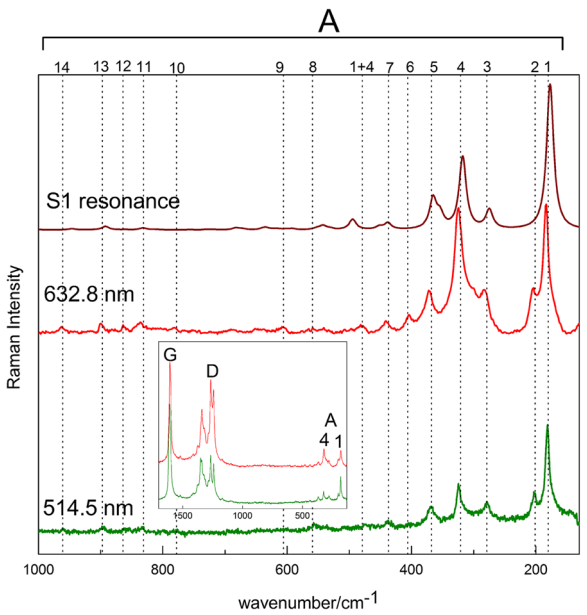

Figure 6. Raman spectra of **C78** in the low wavenumber range recorded with 514.5 nm and 632.8 nm laser excitation.

Table 3. Experimental Raman peaks in the low wavenumber region recorded with 514.5 nm and 632.8 nm laser excitations

		A_1	A_2	A_3	A_4	A_5	A_6	A_7	$A_1 + A_4$	A_8	A_9	A_{10}	A_{11}	A_{12}	A_{13}	A_{14}
Computed wavenum.	A_g	181	—	281	324	373	—	447	505	565	616	790	849	—	911	966
	B_{3g}	—	202	284	—	—	414	—	—	—	—	—	—	874	—	—
Scaled wavenum.		177	198	275 278	317	365	405	438	494	553	603	774	831	856	892	946
Expt. (514.5 nm)		181	203	279	324	368	—	437	477	557	—	776	831	854	898	961
Expt. (632.8 nm)		180	201	281	321	369	401	438	479	556	606	779	833	864	897	960

of the low wavenumber region compared to the G–D region. We have named the Raman signals in this region A_k, after acoustic modes (see Table 3 for the full list). Their nature was already established in the past.[6] The signal-to-noise ratio is remarkably improved compared to previous results,[6] which allows detecting more features than before (mainly A_1 and A_4 were detected). In our analysis we have considered also the Raman signals of the region from 500 cm^{-1} to 1000 cm^{-1} obtained with 514.5 nm and 632.8 nm laser excitations. The use of two excitation wavelengths allows to reliably detecting also the weak features in this spectral region, totaling 15 Raman lines.

The nuclear displacements of the normal modes associated to these peaks can be related to those of in-plane acoustic phonons of a graphene sheet.[6] In particular, it has been shown that the position of A_1 is related to the longitudinal size of a series of PAHs with similar shape as **C78**.[6] The comparison between the experimental spectrum recorded with the 632.8 nm, and the spectrum calculated in perfect resonance with S_1 shows good agreement, which allows assigning the main peaks. The missing peaks in the simulation (A_2, A_6 and A_{12}) are related to non-totally symmetric modes belonging to the B_{3g} irreducible representation. Based on the theory that has been used for evaluating the resonance Raman response,[19,20] the diagonal matrix element of the electron–phonon coupling operator is responsible for Raman scattering (i.e. $< \alpha \mid \partial H/\partial Q_k \mid \alpha >$, with $\mid \alpha >$ being a given excited state electronic wavefunction and $\partial H/\partial Q_k$ the derivative of the electronic Hamiltonian with respect to the normal coordinate Q_k). It can be noticed straightforwardly that this integral vanishes when the normal coordinate Q_k belongs to any non-totally symmetric representation, as it is the case for A_2, A_6 and A_{12}. This implies that the strength of non-totally symmetric modes (e.g. B_{3g}) is zero when evaluating the resonance Raman response with this level of approximation of the theory. The calculation of the Raman intensity of fundamental transitions for non-totally symmetric modes would require the off-diagonal terms $< \alpha \mid \partial H/\partial Q_k \mid \beta >$, which, however, are not straightforwardly evaluated by available TDDFT codes.

Interestingly, it is also possible to observe a peak attributed to the $A_1 + A_4$ combination (see Fig. 6 and Table 3). Compared to the combinations and overtones of G and D peaks, the position of the sum of wavenumber of A_1 and A_4 is more significantly blue shifted with respect to the experimental observation. This may be because of stronger anharmonicity of this lower wavenumber region compared to the CC stretching modes (G, D).

The representation of the nuclear displacements of the first five peaks (A_1 to A_5, whose relative Raman intensity is stronger) is given in Fig. 7, and it is based on results from DFT calculations. Information about the other peaks in this region is available in Supporting Information (Fig. S6 (Supporting Information)).

(c) **Overtones and combinations.** Inspection of the Raman spectrum of **C78** over a wider wavenumber range (150–3500 cm^{-1}, see Fig. 8) reveals the presence of signals that in graphene/graphite systems are attributed to D and G overtones and combinations (i.e. 2D and 2G[8]). These Raman transitions are also predicted by the simulation of the resonance Raman spectrum obtained in perfect resonance condition with the S_1 state, which is compared in Fig. 8 with the spectrum recorded with red excitation at 632.8 nm. The overall agreement between theory and experiment in Fig. 8 is

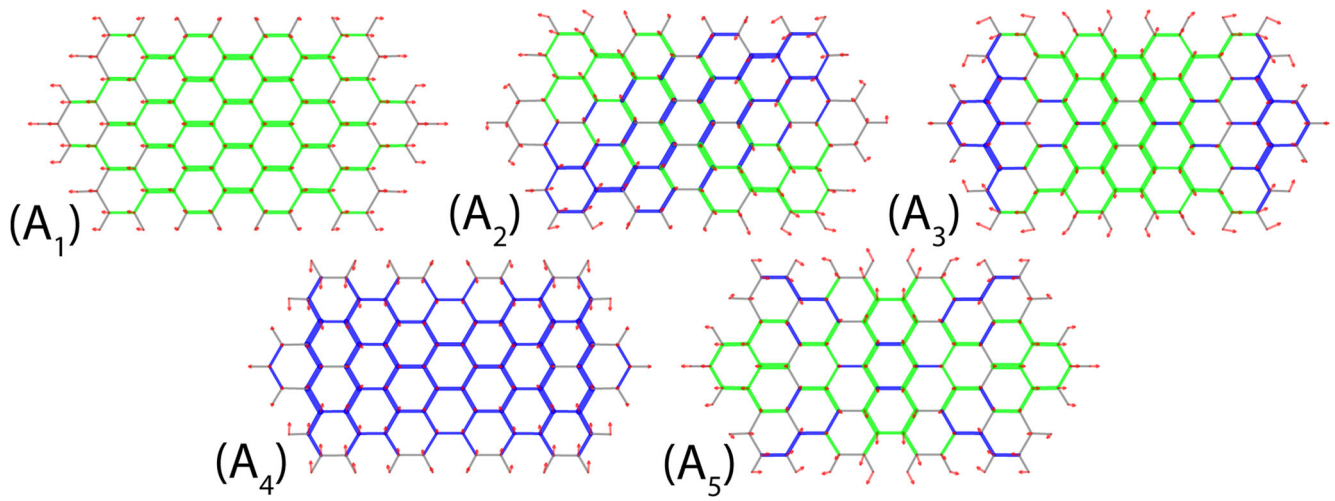

Figure 7. Representation of five most intense collective acoustic-like motion based on computed results from B3LYP/6-31G** calculation. A_1 longitudinal (A_g, 181 cm^{-1}); A_2 shear-like stretching (B_{3g}, 202 cm^{-1}, this mode is absent in the spectrum calculated in perfect resonance with S_1); A_3 collective bending (A_g, 281 cm^{-1}); A_4 transversal stretching (A_g, 324 cm^{-1}); A_5 collective bending (A_g, 373 cm^{-1}). Red arrows represent displacement vectors; CC bonds are represented as green (blue) lines of different thickness according to their relative stretching (shrinking).

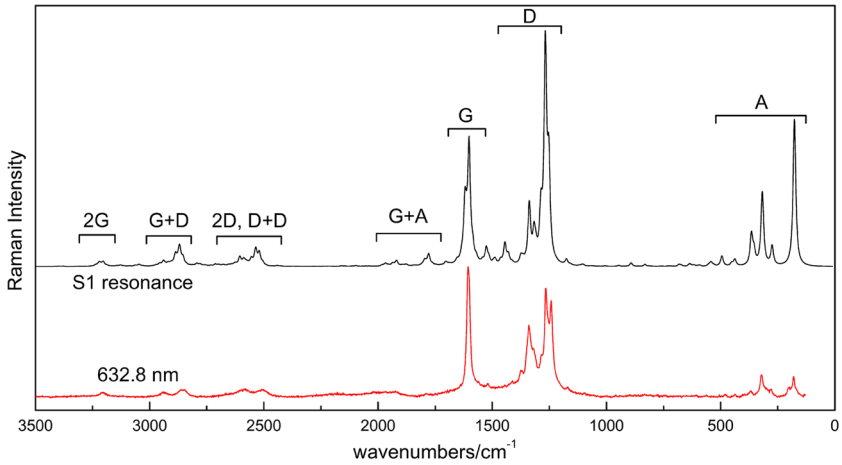

Figure 8. Comparison between calculated S_1 perfect resonance spectrum (black line) with experimental spectrum recorded with 632.8 nm laser excitation (red line).

good. Notably the relative intensity of the A region is overestimated compared to experiment. This is because of the assumption of the perfect resonance condition, which mostly affect the Raman intensities of the lower wavenumber normal modes. Interestingly, **C78** also provides signals which can be attributed to G + D and G + A combinations and which will be described later.

The Raman spectrum of **C78** in the overtone and combination region has been also recorded with excitation lines other than 632.8 nm. These spectra are plotted in Fig. 9. To ease the assessment of the relative intensity of overtones and combinations the G peak is also reported in the Fig. 9. Furthermore, overtones and combinations are also plotted with a 10× magnification factor to help capturing their secondary features. Overall we observe 15 peaks in this region that we label with letters 'a' to 'p' to make a distinction with the labeling scheme adopted for fundamentals. It is possible to distinguish five groups of Raman signals in this region. Based on their wavenumber range, they must be related to 2G overtones, G + D combinations, 2D overtones, $D_j + D_k$ combination and G + A combination. In fact, they match with results from calculations in perfect resonance with S_1 (see Fig. 8 above). In more details, peaks a, b, c, d are related to G + A, peaks e, g, h, j are related to $D_j + D_k$, peaks f, i are related to 2D, peaks k, l, m, n are related to D + G and peak p is related to 2G (see Table 4).

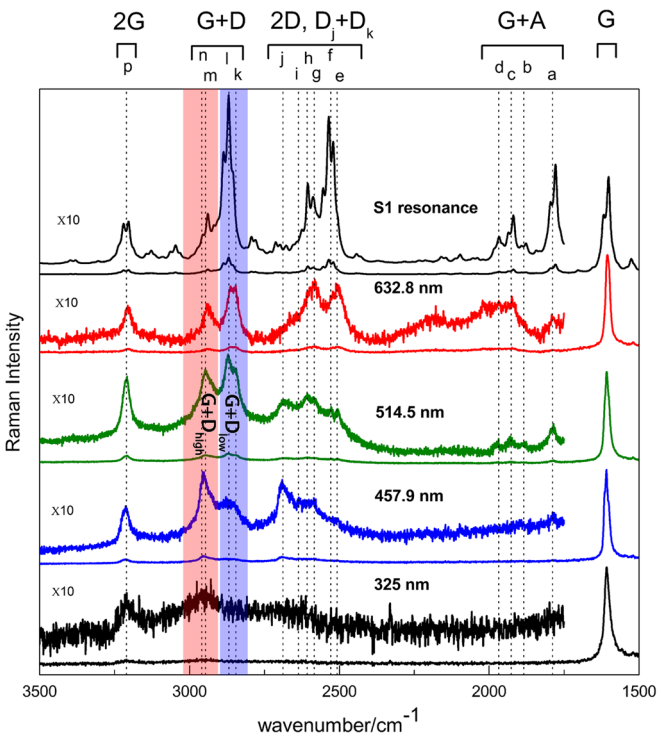

Figure 9. Raman spectra of **C78** in overtone and combination region compared with G peak, recorded with different laser wavelength excitation. For clarity the overtone and combination region has been also plotted overlaid by applying a 10× intensity magnification factor.

Interestingly, according to Ferrari[8] the G + D combination is normally absent in graphene, because of the selection rule based on phonon momentum: the phonon associated to the G peak is found at $\mathbf{q} = \mathbf{0}$, while the phonon associated to the D peak is found at $\mathbf{q} = \mathbf{K} \neq \mathbf{0}$. Hence, the transition associated to the G + D combination would require $\Delta\mathbf{q} \neq \mathbf{0}$. However, G + D combinations are observed in molecular graphenes because for them the phonon wave vector **q** may cease to be an effective quantum number, because of strong confinement over the molecular size. Hence, the intensity of the G + D combination could be used as an experimental measure of phonon confinement effects in graphitic materials. The G + D peak is expected to increase as a consequence of the fact that the **q** wave vector progressively loses its precise meaning as the density of defects increases in the graphitic lattice.

It is also possible to observe four peaks attributable to G + A combinations. In particular, from the analysis of their positions, it turns out that these peaks are related to the combination of the most intense peaks in the A region with the G peak (see Table 4). Interestingly, the G + A_2 combination is *not* observed. This is explained by the fact that A_2 is not totally symmetric (B_{3g}, see Table 3); hence, it cannot combine with any of the strongest components of the G signal, which belong to the totally symmetric representation.

Inspection of Fig. 9 also reveals that, in the overtone and combination region, the relative intensity changes with excitation match the observed behavior of the fundamentals (G, D—see Figs. 4 and 5). This is because of the fact that the Raman intensity of a combination is roughly proportional to the product of the Raman intensities of the corresponding fundamentals. The same holds for overtones too. This can be proved easily by recalling the equations for fundamental Raman transitions[20]

Table 4. Experimental peak position of overtones and combinations recorded with different laser excitations. The proposed assignments are based on the numerical data presented in Tables 1 and 2. When the G peak is involved in the assignment we do not try to identify any specific G component because the experimental signals are too broad to allow reliable peak analysis

	Assignment	325 nm	457.9 nm	514.5 nm	632.8 nm
a	$G + A_1$	—	1788	1786	1791
b	$G + A_3$	—	—	1884	—
c	$G + A_4$	—	—	1929	1924
d	$G + A_5$	—	—	1969	1968
e	$D_2 + D_3$	—	—	2507	2507
f	$2D_3$	—	—	2527	2530
g	$D_2 + D_7$	—	2585	2586	2582
h	$D_3 + D_7$	—	—	2607	2607
i	$2D_6$	—	2636	—	—
j	$D_7 + D_8$	—	2691	2686	—
k	$G + D_2$	—	—	2844	2845
l	$G + D_3$	—	2878	2872	2867
m	$G + D_7$	—	2951	2948	2942
n	$G + D_8$	2961	2957	—	—
p	2G	3210	3213	3209	3206

$$I_h \propto \left(\frac{1}{2\hbar\Omega_h}\right)\left|\frac{\hbar \boldsymbol{g}.\boldsymbol{L}_h}{i\Gamma(i\Gamma+\hbar\Omega_h)}\right|^2 \quad (1)$$

and combinations (the case of overtones is obtained considering the same normal mode index, i.e. $h = k$):

$$I_{h+k} \propto \left(\frac{1}{2\hbar\Omega_h}\right)\left(\frac{1}{2\hbar\Omega_k}\right)\times\left|\frac{(\hbar \boldsymbol{g}.\boldsymbol{L}_h)(\hbar \boldsymbol{g}.\boldsymbol{L}_k)}{i\Gamma(i\Gamma+\hbar\Omega_h)(i\Gamma+\hbar\Omega_h+\hbar\Omega_h)}\right. \quad (2)$$
$$\left.+\frac{(\hbar \boldsymbol{g}.\boldsymbol{L}_k)(\hbar \boldsymbol{g}.\boldsymbol{L}_h)}{i\Gamma(i\Gamma+\hbar\Omega_h)(i\Gamma+\hbar\Omega_h+\hbar\Omega_h)}\right|^2$$

where $\hbar\Omega_k$ represents the vibrational quantum of the k-th normal mode and the scalar product ($\hbar \boldsymbol{g}\cdot\boldsymbol{L}_h$) represents the electron–phonon coupling relative to mode h. The 3 N-components vector $\boldsymbol{g}$ (with N the number of atoms) represents the gradient on the excited state potential energy surface, evaluated with TDDFT methods at the Franck–Condon point. $\boldsymbol{L}_h$ is the 3 N-components vector describing the Cartesian nuclear displacements relative to mode h. Further details can be found in reference.[20] Provided that the resonance broadening parameter Γ is significantly larger than the typical vibrational quantum ($\Gamma \gg \hbar\Omega$), one easily gets from the comparison of Eqn (1) and (2) that $I_{h+k} \propto I_h \times I_k$.

Temperature dependence

We have recorded the Raman spectra of **C78** with 632.8 nm laser excitation over a temperature range extending from 25 °C to 200 °C. As one can see in Fig. 10, the position of G peak shifts to lower wavenumber with increasing temperature. These G peak shifts with temperature have been attributed to thermal expansion phenomena[8] that also affect intermolecular distances and interaction strengths. The position of the three G peak components (by Lorentzian deconvolution, see Fig. S7 (Supporting Information)) markedly red shifts for increasing temperature, as can be clearly observed in Fig. 11. The three components behave fairly similarly and

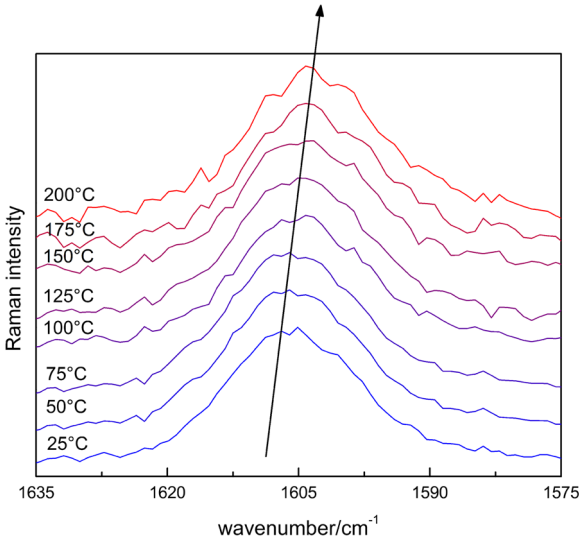

Figure 10. Raman spectra of **C78** over the G region as a function of temperature (632.8 nm excitation).

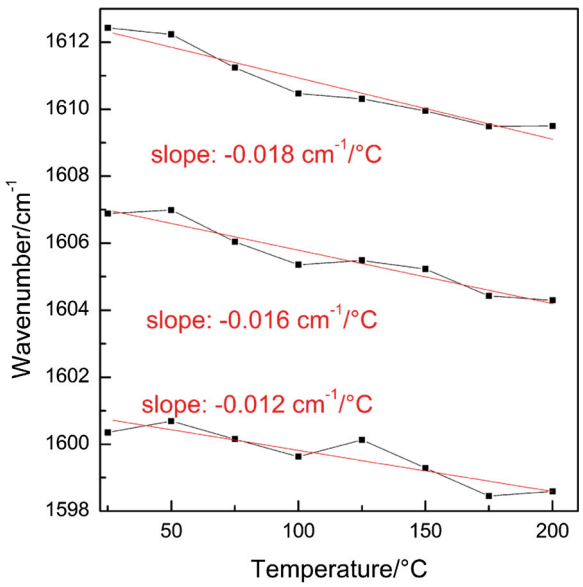

Figure 11. Position of the G peak deconvoluted by three Lorentzian peaks (from the data presented in Fig. 10).

the average slope of the linear dependence of their wavenumber *versus* temperature is $-0.016\ cm^{-1}/°C$.

A qualitatively similar behavior has been measured in graphite by Atashbar,[32] but a different slope was obtained ($-0.031\ cm^{-1}/°C$). Because π–π interactions are expected to be similar in graphite and **C78**, the larger value of graphite may be explained with the additional contribution from phonon-phonon scattering,[32] which is not expected to play a major role in a molecular material such as **C78**.

Conclusions

In this work we report the experimental and theoretical pre-resonance/resonance Raman spectra of **C78**. Compared with a previous investigation[6] the experimental data show better signal-to-noise ratio. More features can be distinguished in the lower wavenumber

region of the spectra, which is associated to in-plane acoustic like vibrations that depend on the molecular size.[6] Moreover, we have extended our analysis to the overtone and combination region (2000–3500 cm^{-1}), which were not explored in the past. We have observed that for selected wavelengths (514.5 and 457.9 nm, which better match resonance conditions) it is possible to observe Raman signals ascribed to 2D and 2G overtones. Furthermore, G + D combinations are also evident in the Raman spectra. This feature is a specific signature of confinement and is usually absent in graphene.[8] The intensity of the G + D combination could be used as an experimental measure of confinement in graphitic materials, and it is expected to increase as a consequence of the fact that the **q** wave vector progressively loses its precise meaning as the density of defects increases in the graphitic lattice.

Finally, we have measured the temperature dependence of the G peak in **C78**, and we have found a linear dependence of $-0.016\ cm^{-1}$/K, because of thermal expansion effects.[8]

References

[1] E. Clar, *The Aromatic Sextet*, Wiley, London, **1972**.
[2] S. Ito, M. Wehmeier, J. Diedrich Brand, C. Kübel, R. Epsch, J. P. Rabe, K. Müllen, *Chem. - Eur. J.* **2000**, *6*, 4327.
[3] W. M. Baird, L. A. Hooven, B. Mahadevan, *Environ. Mol. Mutagen.* **2005**, *45*, 106.
[4] B. T. Draine, A. Li, *Astrophys. J.* **2007**, *657*, 810.
[5] F. Negri, C. Castiglioni, M. Tommasini, G. Zerbi, *J. Phys. Chem. A* **2002**, *106*, 3306.
[6] E. Di Donato, M. Tommasini, G. Fustella, L. Brambilla, C. Castiglioni, G. Zerbi, C. D. Simpson, K. Müllen, F. Negri, *Chem. Phys.* **2004**, *301*, 81.
[7] C. Castiglioni, M. Tommasini, G. Zerbi, *Philos. Trans. R. Soc., A* **2004**, *362*, 2425.
[8] A. C. Ferrari, D. M. Basko, *Nat. Nanotechnol.* **2013**, *8*, 235.
[9] C. Castiglioni, F. Negri, M. Rigolio, G. Zerbi, *J. Chem. Phys.* **2001**, *115*, 3769.
[10] C. Mapelli, C. Castiglioni, G. Zerbi, K. Müllen, *Phys. Rev. B: Condens. Matter Mater. Phys.* **1999**, *60*, 12710.
[11] G. Gouadec, P. Colomban, *Prog. Cryst. Growth Charact. Mater.* **2007**, *53*, 1.
[12] A. K. Geim, K. S. Novoselov, *Nat. Mater.* **2007**, *6*, 183.
[13] A. K. Geim, *Science* **2009**, *324*, 1530.
[14] A. C. Ferrari, J. Robertson, *Phys. Rev. B: Condens. Matter Mater. Phys.* **2000**, *61*, 14095.
[15] R. Escribano, J. J. Sloan, N. Siddique, N. Sze, T. Dudev, *Vib. Spectrosc.* **2001**, *26*, 179.
[16] K. Ohno, *J. Mol. Spectrosc.* **1978**, *72*, 238.
[17] K. Ohno, *J. Chem. Phys.* **1991**, *95*, 5524.
[18] S. Piscanec, M. Lazzeri, F. Mauri, A. C. Ferrari, J. Robertson, *Phys. Rev. Lett.* **2004**, *93*, 185503.
[19] L. A. Nafie, P. Stein, W. L. Peticolas, *Chem. Phys. Lett.* **1971**, *12*, 131.
[20] M. Tommasini, G. Longhi, S. Abbate, G. Zerbi, *J. Raman Spectrosc.* **2014**, *45*, 89.
[21] M. D. Watson, A. Fechtenkötter, K. Müllen, *Chem. Rev. (Washington, DC, U. S.)* **2001**, *101*, 1267.
[22] G. M. Rutter, N. P. Guisinger, J. N. Crain, P. N. First, J. A. Stroscio, *Phys. Rev. B: Condens. Matter. Phys.* **2010**, *81*, 245408.
[23] P. Egberts, G. H. Han, X. Z. Liu, A. T. C. Johnson, R. W. Carpick, *ACS Nano* **2014**, *8*, 5010.
[24] J. M. Wofford, S. Nie, K. F. McCarty, N. C. Bartelt, O. D. Dubon, *Nano Lett.* **2010**, *10*, 4890.
[25] Z. Luo, S. Kim, N. Kawamoto, A. M. Rappe, A. T. C. Johnson, *ACS Nano* **2011**, *5*, 9154.
[26] Y. Son, M. L. Cohen, S. G. Louie, *Phys. Rev. Lett.* **2006**, *97*, 216803.
[27] K. A. Ritter, J. W. Lyding, *Nat. Mater.* **2009**, *8*, 235.
[28] M. J. Frisch, G. W. Trucks, H. B. Schlegel, G. E. Scuseria, M. A. Robb, J. R. Cheeseman, G. Scalmani, V. Barone, B. Mennucci, G. A. Petersson, H. Nakatsuji, M. Caricato, X. Li, H. P. Hratchian, A. F. Izmaylov, J. Bloino, G. Zheng, J. L. Sonnenberg, M. Hada, M. Ehara, K. Toyota, R. Fukuda, J. Hasegawa, M. Ishida, T. Nakajima, Y. Honda, O. Kitao, H. Nakai, T. Vreven, J. A. Montgomery Jr., J. E. Peralta, F. Ogliaro, M. Bearpark, J. J. Heyd, E. Brothers, K. N. Kudin, V. N. Staroverov, R. Kobayashi, J. Normand, K. Raghavachari, A. Rendell, J. C. Burant, S. S. Iyengar, J. Tomasi, M. Cossi, N. Rega, J. M. Millam, M. Klene, J. E. Knox, J. B. Cross, V. Bakken, C. Adamo, J. Jaramillo, R. Gomperts, R. E. Stratmann, O. Yazyev, A. J. Austin, R. Cammi, C. Pomelli, J. W. Ochterski, R. L. Martin, K. Morokuma, V. G. Zakrzewski, G. A. Voth, P. Salvador, J. J. Dannenberg, S. Dapprich, A. D. Daniels, Ö. Farkas, J. B. Foresman, J. V. Ortiz, J. Cioslowski, D. J. Fox, *Gaussian 09, Revision D.01*, Gaussian, Inc., Wallingford CT, **2009**.
[29] F. J. Avila Ferrer, V. Barone, C. Cappelli, F. Santoro, *J. Chem. Theory Comput.* **2013**, *9*, 3597.
[30] I. Childres, L. A. Jauregui, Y. P. Chen, *J. Appl. Phys. (Melville, NY, U. S.)* **2014**, *116*, 233101.
[31] I. Pócsik, M. Hundhausen, M. Koós, L. Ley, *J. Non-Cryst. Solids* **1998**, *227–230*, 1083.
[32] M. Z. Atashbar, S. Singamaneni, *Appl. Phys. Lett.* **2005**, *86*, 123112.
[33] M. Sun, Z. Zhang, L. Chen, H. Xu, *Adv. Opt. Mater.* **2013**, *25*, 449.

Supporting information

Additional supporting information may be found in the online version of this article at the publisher's website.